

Thermal and athermal components in strain hardening of martensite

L.Y. Wang¹, Y.X. Wu¹, W.W. Sun^{1,2}, Y. Bréchet¹, L. Brassart^{1,3}, A. Arlazarov⁴, C.R. Hutchinson^{1*}

¹ Department of Materials Science and Engineering, Monash University, Clayton, VIC 3800, Australia

² School of Materials Science and Engineering, Southeast University, Nanjing 211189, China

³ Department of Engineering Science, University of Oxford, Oxford OX1 3PJ, United Kingdom

⁴ ArcelorMittal Global Research and Development, Voie Romaine-BP30320, 57283, Maizières-les-Metz,
France

*Corresponding Author: christopher.hutchinson@monash.edu

Keywords: Martensite, tempered martensite, Bauschinger test, strain-rate sensitivity, athermal hardening, kinematic hardening.

Abstract

Recent theories consider as-quenched martensite as a composite which strain hardens by the gradual yielding of constituents. An underlying hypothesis is that hardening comes primarily from athermal hardening contributions. In this contribution, we conducted strain-rate jump and tension-compression tests to quantify the athermal and kinematic hardening contributions in martensite. It is shown that athermal hardening accounts for ~75% of the total strength of as-quenched martensite. The magnitudes of athermal and kinematic hardening decrease as a function of tempering. A correlation between the athermal and kinematic hardening contributions is identified and shown to be independent of chemistry and tempering condition.

Strain hardening of as-quenched martensite has drawn renewed interests in the community thanks to its application in advanced high strength steels (AHSS). Recent models propose that the high strain hardening rate of as-quenched martensite comes from the gradual yielding of microstructural constituents having variations in either intrinsic yield stresses [1] or transformation induced residual stresses [2,3]. Modelling results from these composite hypotheses show good agreement with experimental data without considering strain hardening from multiplication and entanglement of forest dislocations [4–6]. By nature, dislocation based strain hardening is isotropic and has a thermal dependence because of thermally activated dislocation glide and dynamic recovery [7]. Strain hardening from the composite effect, on the other hand, is more athermal and kinematic as a result of long-range interactions between dislocations and large obstacles [8,9]. The magnitude of athermal hardening in as-quenched martensite have not been quantified experimentally in previous works. Questions also remain in the case of tempered martensite where the microstructure of the initial as-quenched martensite recovers and the strain hardening rate decreases [10,11]. To verify this key hypothesis of the composite models, we conducted strain-rate jump and tension-compression tests to investigate the magnitude of the athermal and kinematic hardening contributions in as-quenched and tempered martensite.

The materials used in this study were provided by ArcelorMittal and their compositions are shown in Table 1. The base composition is Fe-0.25C-2.5Mn (mass%). Si and Al were added to study the alloying element effect. The steels have been provided as both cold rolled (CR) sheets (~1.2 mm thick) and hot rolled (HR) plates (~6 mm thick). The cold rolled sheets were used for strain-rate jump tests and the hot rolled plates were used to perform tension-compression tests. The austenitisation experiments were conducted in a horizontal tube furnace heated to 950°C with flowing Ar for 10 minutes followed by water quenching. The tempering experiments were performed in a salt bath (300°C – 600°C) for 5 minutes and 1 hour to capture the short-time and long-time behaviours at each temperature.

Table 1 The chemical compositions of the investigated steels (mass%)

Designation (reference composition)		Fe	C	Mn	Si	Al	P	S
Base steel (Fe-0.25C-2.5Mn)	CR	Bal.	0.24	2.4	<0.02	0.01	0.01	0.01
	HR	Bal.	0.25	2.43	<0.02	0.01	0.01	0.01
Si steel (Fe-0.25C-2.5Mn-1.4Si)	CR	Bal.	0.25	2.42	1.44	0.01	0.01	0.01
	HR	Bal.	0.24	2.4	1.45	0.01	0.01	0.01
Al steel (Fe-0.25C-2.5Mn-1.4Al)	CR	Bal.	0.27	2.46	0.02	1.38	0.01	0.01
	HR	Bal.	0.26	2.52	0.02	1.42	0.01	0.01

Samples with a gauge length of 12 mm and a gauge width of 5 mm were electrodischarge machined from the cold rolled sheets parallel to the rolling direction. The strain-rate jump tests were performed using a servo-hydraulic MTS Landmark machine with a 100 kN load capacity. The crosshead speed during the initial ramp was fixed at 0.002 mm/s (equivalent strain-rate $\sim 1.67 \times 10^{-4} \text{ s}^{-1}$) until 0.5% total strain was reached. Crosshead speed jumps were then performed every 0.5% between 0.002 mm/s and 0.02 mm/s, which results in $\dot{\epsilon}_1/\dot{\epsilon}_2 = 10$ or 0.1. The change in flow stress $\Delta\sigma$ after a strain-rate jump event was determined as the instantaneous change in the true stress during a down-jump (i.e. from high strain-rate to low strain-rate). The down-jump was chosen since it displays smaller noise compared to the up-jump (i.e. from low strain-rate to high strain-rate).

Analyses of the strain-rate sensitivity test followed the approach of Kocks *et al.* [7] and Mulford [12]. The activation area Δa during thermally activated dislocation motion can be expressed as:

$$\Delta a = -\frac{1}{b} \frac{\partial \Delta G}{\partial \tau} \quad (1)$$

where b is the Burgers vector, ΔG is the activation energy and τ is the applied shear stress. If we define the shear strain-rate with an Arrhenius behaviour $\dot{\gamma} = \dot{\gamma}_0 \exp(-\Delta G/kT)$ and define the strain-rate sensitivity parameter $m = \partial \ln \dot{\gamma} / \partial \ln \tau$, the activation area can be related to the strain-rate sensitivity by:

$$\Delta a = \frac{MmkT}{b\sigma} \quad (2)$$

where M is the Taylor factor that converts the flow stress σ to shear components and k is Boltzmann's constant [13]. If the material is only strengthened by forest dislocations, the plot of $1/\Delta a$ against σ (Haasen plot) should be linear and can be extrapolated to the origin (i.e. satisfying the Cottrell-Stokes law [14]). If the material is strengthened by other types of obstacles that are more athermal than forest dislocations, the curve may have a non-zero intercept with the stress axis. In this contribution, we will use the x-intercept on the Haasen plot as an estimation for athermal contributions. The magnitude of the thermal contributions will be estimated by the difference between the athermal contributions and the experimental ultimate tensile strength (UTS) which is measured prior to the strain-rate jump tests.

Figure 1 shows the Haasen plot of as-quenched and tempered martensite. In the case of as-quenched martensite (Figure 1a, c and e), while the first few data points on the Haasen plot do not perfectly obey the Cottrell-Stokes law, the points obtained close to the UTS can be fitted well by linear regressions. Regardless of the alloy composition, a single slope can be used for the linear regressions and the fitted lines have large intercepts with the stress axis. According to the physical construction of the Haasen plot, the thermal contribution should only come from forest dislocations [7,12]. Our results suggest that the athermal contribution to the flow strength of as-quenched martensite accounts for $\sim 75\%$ of the UTS (x-intercepts divided by the experimental UTS). This agrees with the implicit hypothesis made in the composite strengthening models that the dislocation-based mechanism is not the dominant strengthening mechanism in as-quenched martensite.

In the case of tempered martensite, the same slope used in the as-quenched state was used to describe the evolution of the inversely normalised activation area ($b^2/\Delta a$) in tempered samples. Although some discrepancies may be found in the 600°C tempered samples, the overall fit between the linear regression and the experimental data show good agreement regardless of chemical composition and tempering condition. This indicates that the alloy chemistry and tempering conditions (time and temperature), have a relatively small effect on the dislocation storage in martensite until reaching the heavily tempered states. However, tempering does reduce the magnitude of athermal hardening which is shown as the shift of x-intercepts to lower stress values.

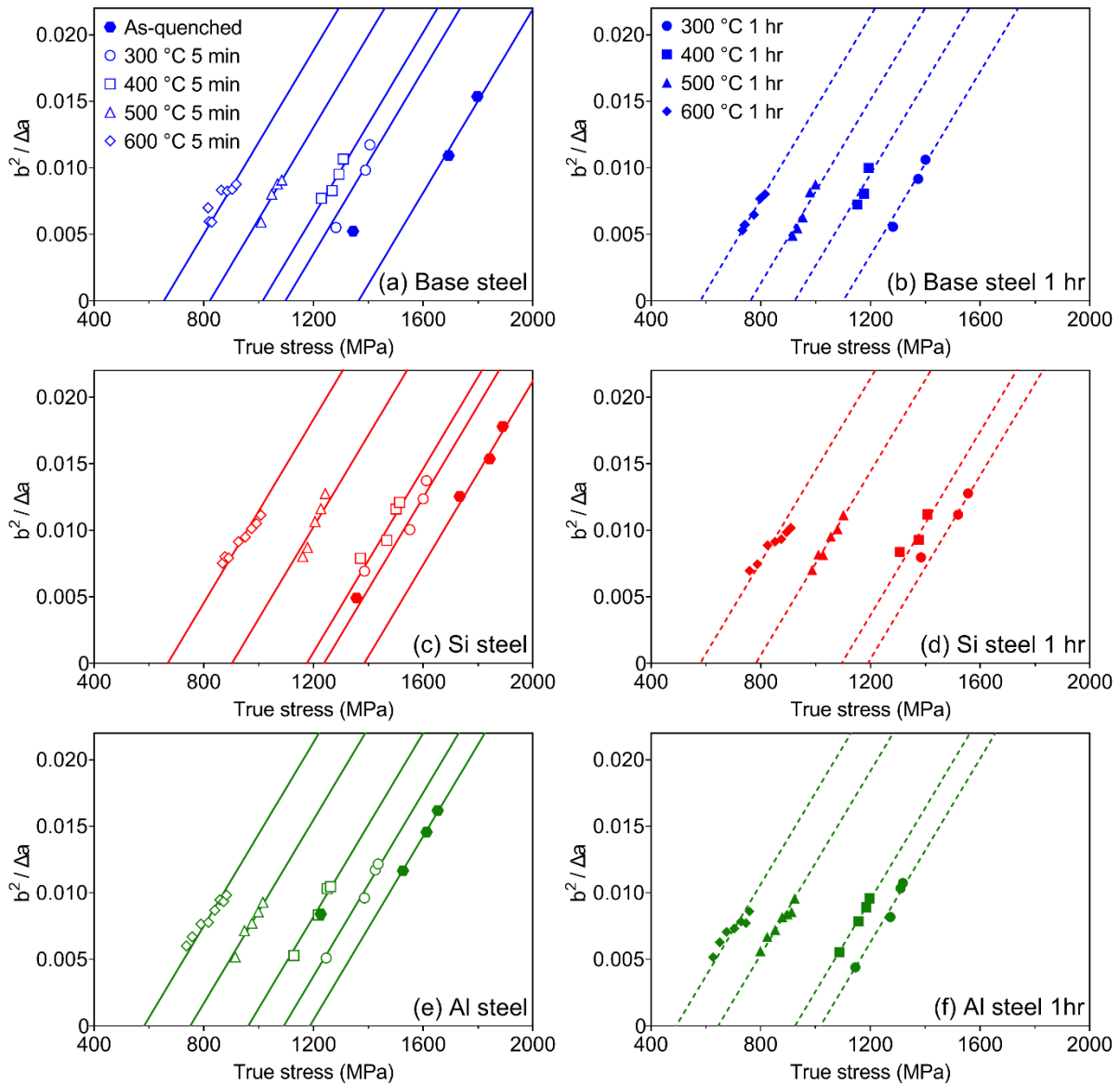


Figure 1 Haasen plots of the base steel (a - b), the Si steel (c - d) and the Al steel (e - f) tempered at different temperatures for 5 minutes and 1 hour. The error in the estimation of the instantaneous stress change is 0.5 – 1 MPa, resulting in uncertainties around 5% - 10% in the estimation of Δa .

Athermal contributions to the flow stress arise from dislocation interactions with obstacles that are less susceptible to thermal activation than forest dislocations. In the case of as-quenched martensite, plastic incompatibilities and dislocation-obstacle interactions (e.g. grain boundaries and precipitates) should be the dominant contributions as a result of the heterogeneous and hierarchical microstructure [15–19]. Theoretically, both mechanisms should lead to the continuous development of athermal hardening during straining and contribute to the strain hardening of the material. While the strain-rate jump test gives an estimation of the total contribution from athermal hardening, tension-compression Bauschinger tests can be used to monitor the development of the athermal, kinematic hardening contribution.

Tension-compression tests were conducted using a servo-hydraulic MTS Landmark machine with a 100 kN capacity. The alignment of the testing system was calibrated to be close to ASTM E1012 Class 5 using the MTS 609 alignment fixture and a standard sample with 12 strain gauges before each set of tests. Samples with a gauge length of 18 mm and a gauge diameter of 4.5 mm were machined from the HR plates with their longitudinal directions parallel to the rolling direction. Tension-compression tests were conducted with a constant crosshead speed of 0.03 mm/s (equivalent strain-rate $\sim 1.67 \times 10^{-3} \text{ s}^{-1}$) and two clip-on extensometers mounted diametrically opposed to each other were used to measure the extension of the gauge section. This setup was used so that buckling during compression can be identified when the readings from the two extensometers deviate from each other significantly [20–22]. The back stress σ_b (kinematic hardening) can be calculated as:

$$\sigma_b = \frac{\sigma_f - |\sigma_r|}{2} \quad (3)$$

where σ_f is the flow stress at the end of the forward loading and σ_r is the offset yield stress during reverse loading. The magnitude of σ_b depends on the choice of the reverse strain offset in determining σ_r [20–22]. In this work, we used an offset of 0.2% which is commonly found in the literature of steels [23–26]. For each tempering condition, several forward strains were chosen and the maximum forward strain was set approximately 0.5% to 1% below the uniform elongation. This ensures the maximum back stress could be measured without the complication of strain localisation due to necking at the UTS.

Figure 2 shows the evolution of back stress as a function of forward plastic strains. The continuous lines are obtained by fitting the experimental back stress data with the phenomenological non-linear kinematic hardening model ($\sigma_b = 2/3 \cdot C_\xi / \xi \cdot \exp(-\xi \varepsilon_p)$), where C_ξ describes the effective hardening modulus and ξ takes into account the dynamic recovery of hardening) [27]. In general, the fitted lines can describe well the evolution of the back stress as a function of plastic strain. In the case of as-quenched martensite, the back stress starts small and quickly develop during straining and the maximum back stress obtained near the UTS accounts for $\sim 27\%$ of the total flow stress and $\sim 40\%$ of the total athermal hardening contribution regardless of alloy composition. It indicates that kinematic hardening developed during straining has a non-trivial contribution to athermal hardening and the macroscopic strength of as-quenched martensite.

Similar to the athermal contribution, the back stress also decreases after tempering. It can be seen that tempering does not only reduce the magnitude of the back stress but also affects the rate of development. As tempering proceeds, the kinematic hardening rates at high plastic strains decrease and eventually become relatively flat after tempering above 500°C. This implies that there could be a transition in the mechanism that governs the kinematic hardening. Literature data has demonstrated that the strain hardening rate in high temperature (> 500°C) tempered martensite is much smaller compared to the as-quenched and low temperature tempered martensite [10,11]. Therefore, the composite strengthening hypothesis may not be suitable for high temperature tempering and requires other strain hardening mechanisms to be introduced. Indeed, modelling results from Kim *et al.* [17] and Chang and Asaro [18] also suggest that the back stress generated in high temperature tempered martensite can be rationalised by considering kinematic hardening originated at grain boundaries or cementite precipitates.

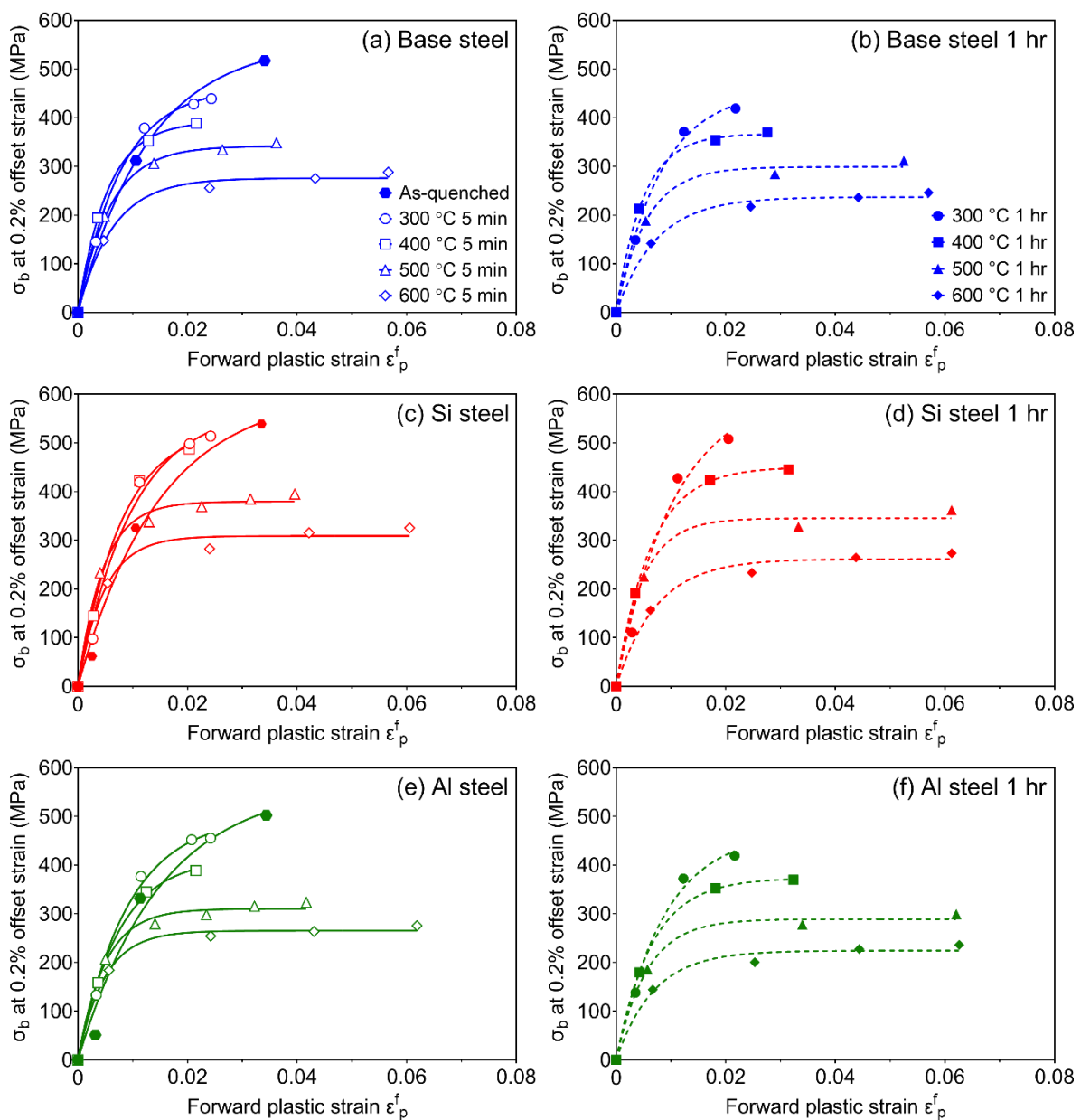


Figure 2 Evolution of back stresses as a function of forward plastic strains of the base steel (a - b), the Si steel (c - d) and the Al steel (e - f) tempered at different temperatures for 5 minutes and 1 hour. The uncertainty associated with the back stress is around 10 – 30 MPa due to sample to sample differences.

Figure 3 compares the athermal (Figure 3a) and kinematic (Figure 3b) hardening contribution. The x-axis here represents the tempering parameter proposed by Hollomon and Jaffe which allows data from different tempering temperatures and times to be plotted on the same graph [28]. The athermal hardening contributions decrease continuously as a function of tempering and the addition of Si retards the kinetics of the reduction. The thermal hardening contributions, calculated as the difference between the UTS and the athermal stress, remain relatively constant and the reduction from the as-quenched state is approximately 200 MPa for all compositions after tempering at 300°C. This suggests that while the decrease in dislocation-based thermal stresses contributes to the softening of martensite, a large proportion of softening should be attributed to the reduction of athermal hardening contributions. The evolution of the maximum back stress also shows a similar trend to the evolution of the athermal hardening contribution where the addition of Si slows the decrease in the back stress. Therefore, the softening of martensite can be largely attributed to the reduction in the athermal and kinematic hardening contributions.

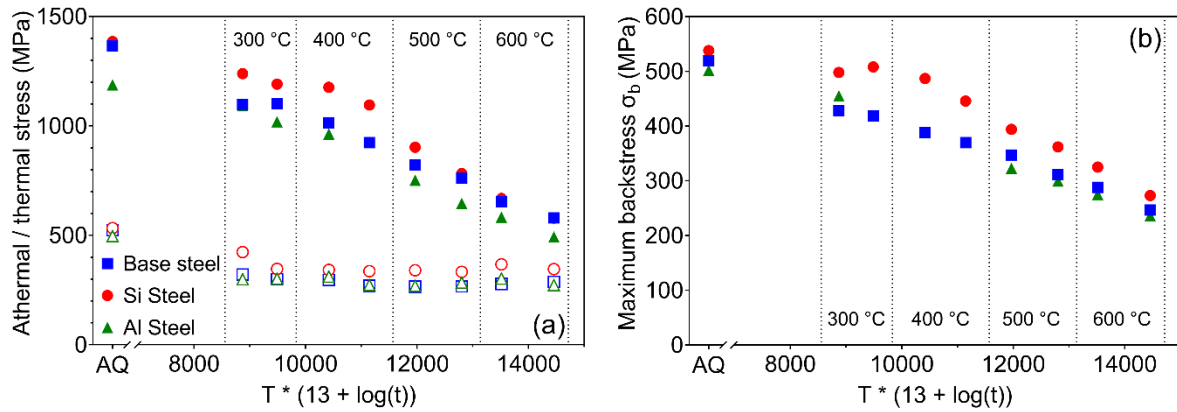


Figure 3 Quantification of athermal and kinematic hardening contributions. (a) Hollomon-Jaffe plot showing the evolution of athermal (solid symbols) and thermal (open symbols) hardening contributions. (b) Hollomon-Jaffe plot showing the evolution of the maximum back stresses. At each temperature, two tempering times are shown (i.e. 5 minutes and 1 hour).

Since both the athermal hardening and the kinematic hardening contributions originate from long-range internal stresses developed during straining, it is worth exploring if they are correlated in the martensite system. Figure 4 shows the correlation between the maximum back stress and the athermal stress in all samples (both as-quenched and tempered). A master curve can be fitted to all compositions for all tempering conditions, which suggests that the correlation is not strongly altered by the addition of Si and Al regardless of their effects on the softening kinetics. The slope of the correlation depends on the offset strain used in the back stress estimation but the magnitude of the slope does not become one even if a smaller offset (0.1%) is chosen. This implies that the magnitude of kinematic hardening is always smaller than the magnitude of athermal hardening and kinematic hardening accounts for approximately the same fraction of athermal hardening throughout

tempering. Both experimental and modelling works are required to examine if kinematic hardening is indeed always smaller than athermal hardening, and not from artefacts associated with the reverse offset.

It is worth noting that this master curve has a non-zero intercept with the back stress axis and the magnitude of the intercept is not sensitive to the selection of the offset strain (~60 - 70 MPa). This suggests that even if the material is predominantly strengthened by forest dislocations, the kinematic hardening contribution does not necessarily go to zero. One example to support this hypothesis can be found in the test results of interstitial free (IF) steels. Bouaziz *et al.* [29] performed shear reversal tests on sheet IF steel samples and found that the maximum magnitude of the back stress is ~30 MPa and it could be attributed to the development of dislocation cell structures during plastic straining [30]. It agrees reasonably well with the y-intercept in Figure 4 considering the vast differences between martensite and IF steel microstructures.

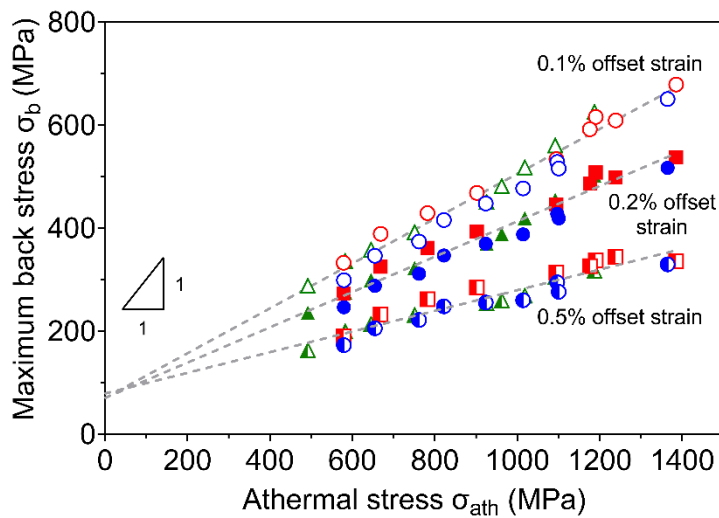


Figure 4 The correlation between the maximum back stress obtained from Bauschinger tests and the athermal stress obtained from strain rate jump tests. Dashed lines are fitted with linear regressions with different slopes. The triangle represents the slope for a one-to-one ratio.

The existence correlation between the athermal and kinematic hardening contributions that is independent of chemistry and tempering conditions, also indicates that the back stress obtained from Bauschinger tests may be estimated by the athermal hardening obtained using strain-rate jump tests. While the slope of this correlation may be different in other alloy classes (e.g. Cu and Al alloys), it can be useful in estimating the magnitude of the back stress (and the Bauschinger effect) when the test samples are not suitable for a tension-compression test (such as sheet samples).

In summary, the experimental results from strain-rate jump and tension-compression tests support the hypothesis in composite models that athermal and kinematic hardening dominate the flow stress of as-quenched martensite. In the case of tempered martensite, the magnitude of the athermal and kinematic hardening contributions decrease as tempering proceeds. A correlation is found between the athermal and kinematic hardening contributions that is independent of alloy chemistry and tempering state. This can reduce the experimental complexity in estimating the Bauschinger effect in other materials.

Acknowledgments

The authors would like to thank the support of ArcelorMittal and the Australian Research Council through the Linkage Grant Scheme (LP150100756). YXW and LYW gratefully acknowledges the award of the Australian Government Research Training Program.

References

- [1] S. Allain, O. Bouaziz, M. Takahashi, Toward a New Interpretation of the Mechanical Behaviour of As-quenched Low Alloyed Martensitic Steels, *ISIJ Int.* 52 (2012) 717–722. doi:10.2355/isijinternational.52.717.
- [2] B. Hutchinson, D. Lindell, M. Barnett, Yielding Behaviour of Martensite in Steel, *ISIJ Int.* 55 (2015) 1114–1122. doi:10.2355/isijinternational.55.1114.
- [3] B. Hutchinson, P. Bate, D. Lindell, A. Malik, M. Barnett, P. Lynch, Plastic yielding in lath martensites – An alternative viewpoint, *Acta Mater.* 152 (2018) 239–247. doi:10.1016/j.actamat.2018.04.039.
- [4] S. Takaki, K.-L. Ngo-Huynh, N. Nakada, T. Tsuchiyama, Strengthening Mechanism in Ultra Low Carbon Martensitic Steel, *ISIJ Int.* 52 (2012) 710–716. doi:10.2355/isijinternational.52.710.
- [5] D. Akama, T. Tsuchiyama, S. Takaki, Change in Dislocation Characteristics with Cold Working in Ultralow-carbon Martensitic Steel, *ISIJ Int.* 56 (2016) 1675–1680. doi:10.2355/isijinternational.ISIJINT-2016-140.
- [6] T. Swarr, G. Krauss, The effect of structure on the deformation of as-quenched and tempered martensite in an Fe-0.2 pct C alloy, *Metall. Trans. A.* 7 (1976) 41–48. doi:10.1007/BF02644037.
- [7] U.F. Kocks, A.S. Argon, M.F. Ashby, Thermodynamics and Kinetics of Slip, *Prog. Mater. Sci.* 19 (1975) 1.
- [8] R.J. Asaro, Elastic-Plastic Memory and Kinematic Type Hardening, *Acta Metall.* 23 (1975) 1255–1265.
- [9] V. Schulze, O. Vöhringer, Plastic Deformation: Constitutive Description, in: *Encycl. Mater. Sci. Technol.*, Elsevier, 2001: pp. 7050–7064. doi:10.1016/B0-08-043152-6/01250-X.
- [10] G. Krauss, Tempering of Lath Martensite in Low and Medium Carbon Steels: Assessment and Challenges, *Steel Res. Int.* 87 (2017) 1700038. doi:10.1002/srin.201700038.
- [11] L.R. Cupertino Malheiros, E.A. Pachon Rodriguez, A. Arlazarov, Mechanical behavior of tempered martensite: Characterization and modeling, *Mater. Sci. Eng. A.* 706 (2017) 38–47. doi:10.1016/j.msea.2017.08.089.
- [12] R.A. Mulford, Analysis of strengthening mechanisms in alloys by means of thermal-activation theory, *Acta Metall.* 27 (1979) 1115–1124. doi:10.1016/0001-6160(79)90129-9.
- [13] G.C. Kaschner, J.C. Gibeling, Evolution of dislocation glide kinetics during cyclic deformation of copper, *Acta Mater.* 50 (2002) 653–662. doi:10.1016/S1359-6454(01)00362-7.
- [14] A.H. Cottrell, R.J. Stokes, Effects of temperature on the plastic properties of aluminium crystals, *Proc. R. Soc. London. Ser. A. Math. Phys. Sci.* 233 (1955) 17–34. doi:10.1098/rspa.1955.0243.
- [15] S. Morito, H. Tanaka, R. Konishi, T. Furuhashi, T. Maki, The morphology and crystallography of lath martensite in Fe-C alloys, *Acta Mater.* 51 (2003) 1789–1799. doi:10.1016/S1359-6454(02)00577-3.

- [16] J.L. Zhang, L. Morsdorf, C.C. Tasan, Multi-probe microstructure tracking during heat treatment without an in-situ setup: Case studies on martensitic steel, dual phase steel and β -Ti alloy, *Mater. Charact.* 111 (2016) 137–146. doi:10.1016/j.matchar.2015.11.019.
- [17] B. Kim, E. Boucard, T. Sourmail, D. San Martin, N. Gey, P.E.J. Rivera-Diaz-Del-Castillo, The influence of silicon in tempered martensite: Understanding the microstructure-properties relationship in 0.5-0.6 wt.% C steels, *Acta Mater.* 68 (2014) 169–178. doi:10.1016/j.actamat.2014.01.039.
- [18] Y.W. Chang, R.J. Asaro, Bauschinger effects and work-hardening in spheroidized steels, *Met. Sci.* 12 (1978) 277–284. doi:10.1179/030634578790433756.
- [19] S. Cobo, O. Bouaziz, Investigations and Modelling of the Work Hardening of As-Quenched Martensite, in: *New Dev. Metall. Appl. High Strength Steels*, Buenos Aires 2008 - Proc. Int. Conf. New Dev. Metall. Appl. High Strength Steels, 2008: pp. 909–918.
- [20] S.F. Corbin, D.S. Wilkinson, J.D. Embury, The Bauschinger effect in a particulate reinforced Al alloy, *Mater. Sci. Eng. A.* 207 (1996) 1–11. doi:10.1016/0921-5093(95)10028-8.
- [21] J. da Costa Teixeira, L. Bourgeois, C.W. Sinclair, C.R. Hutchinson, The effect of shear-resistant, plate-shaped precipitates on the work hardening of Al alloys: Towards a prediction of the strength-elongation correlation, *Acta Mater.* 57 (2009) 6075–6089. doi:10.1016/j.actamat.2009.08.034.
- [22] G. Badinier, C.W. Sinclair, S. Allain, O. Bouaziz, The Bauschinger effect in drawn and annealed nanocomposite Cu-Nb wires, *Mater. Sci. Eng. A.* 597 (2014) 10–19. doi:10.1016/j.msea.2013.12.031.
- [23] M.D. Richards, C.J. Van Tyne, D.K. Matlock, The influence of dynamic strain aging on resistance to strain reversal as assessed through the Bauschinger effect, *Mater. Sci. Eng. A.* 528 (2011) 7926–7932. doi:10.1016/j.msea.2011.07.015.
- [24] L. Zhonghua, G. Haicheng, Bauschinger Effect and Residual Phase Stresses in Two Ductile-Phase Steels : Part II . The Effect of Microstructure and Mechanical Properties of the Constituent Phases on Bauschinger Effect and Residual Phase Stresses, *Metall. Trans. A.* 21 (1990) 725–732.
- [25] K. Han, C.J. Van Tyne, B.S. Levy, Bauschinger effect response of automotive sheet steels, *SAE Trans. J. Mater. Manuf.* 114 (2005) 27–33.
- [26] K. Han, C.J. Van Tyne, B.S. Levy, Effect of strain and strain rate on the bauschinger effect response of three different steels, *Metall. Mater. Trans. A.* 36 (2005) 2379–2384.
- [27] J.L. Chaboche, A review of some plasticity and viscoplasticity constitutive theories, *Int. J. Plast.* 24 (2008) 1642–1693. doi:10.1016/j.ijplas.2008.03.009.
- [28] J.H. Hollomon, Tensile Deformation, *Trans. Metall. Soc. AIME.* 162 (1945) 268–290.
- [29] O. Bouaziz, D. Barbier, J.D. Embury, G. Badinier, An extension of the Kocks-Mecking model of work hardening to include kinematic hardening and its application to solutes in ferrite, *Philos. Mag.* 93 (2013) 247–255. doi:10.1080/14786435.2012.704419.
- [30] E.F. Rauch, J.J. Gracio, F. Barlat, Work-hardening model for polycrystalline metals under strain reversal at large strains, *Acta Mater.* 55 (2007) 2939–2948. doi:10.1016/j.actamat.2007.01.003.